Global and pixel kinetic data analysis for FRET detection by multi-photon time-domain FLIM

P. R. Barber*, S. M. Ameer-Beg, J. Gilbey, R. J. Edens, I. Ezike, B. Vojnovic.
Gray Cancer Institute, Mount Vernon Hospital, Northwood, Middlesex, HA6 2JR

ABSTRACT

FLIM/FRET is an extremely powerful technique that can microscopically locate nanometre-scale protein-protein interactions within live or fixed cells, both *in vitro* and *in vivo*. The key to performing sensitive FRET, via FLIM, besides the use of appropriate fluorophores, is the analysis of the time-resolved data present at each image pixel. The fluorescent transient will, in general, exhibit multi-exponential kinetics: at least two exponential components arise from both the interacting and non-interacting protein. We shall describe a novel method and computer program for the global analysis of time resolved data, either at the single level or through global analysis of grouped pixel data. Kinetic models are fitted using the Marquardt algorithm and iterative convolution of the excitation signal, in a computationally-efficient manner. The fitting accuracy and sensitivity of the algorithm has been tested using modelled data, including the addition of simulated Poisson noise and repetitive excitation pulses which are typical of a TCSPC system.
We found that the increased signal to noise ratio offered by both global and invariance fitting is highly desirable. When fitting mono-exponential data, the effects of a *ca.*12.5 ns (*ca.* 80 MHz) repetitive excitation do not preclude the accurate extraction of populations with lifetimes in the range 0.1 to 10 ns, even when these effects are not represented in the fitting algorithm. Indeed, with global or invariance fitting of a 32x32 pixel area, the error in extracted lifetime can be lower than 0.4 % for signals with a peak of 500 photon counts or more. In FRET simulations, modelling GFP with a non-interacting lifetime of 2.15 ns, it was possible to accurately detect a 10 % interacting population with a lifetime of 0.8 ns.

Keywords: Time-resolved microscopy, TCSPC, FLIM, FRET, kinetic fitting, global analysis

1. INTRODUCTION

Detecting protein-protein interactions within a biological cell will lead to a greater understanding of the key mechanisms that regulate the fundamental processes of the cell. There is a particular advantage to locating these interactions both spatially and temporally when we study cells *in situ* and, in particular, *in vivo*. When these interactions occur, the separation distance between proteins can be of the order of a few nanometres. One experimental technique which is sensitive at these small scales, the so called 'near field', is the detection of fluorescence resonance energy transfer (FRET). FRET can be detected optically if the proteins are conjugated with suitable fluorophores.
The efficiency of energy transfer between these fluorophores (coupling efficiency) varies as the inverse-sixth power of the distance between acceptor and donor. It is typically described in terms of the Förster radius (distance at which the efficiency of energy transfer is 50%), which is usually of the order 1-10 nm. The process depletes the excited state population of the donor reducing the fluorescence intensity and the fluorescence lifetime of the donor. The advantage of using donor fluorescence lifetime to detect FRET via fluorescence lifetime imaging microscopy (FLIM), is the independence of the measurement to fluorophore concentration and to light path length. It is therefore well suited to studies in intact cells[1,2]. Combining this with confocal or multiphoton microscopy to examine the localisation of effects in cellular compartments, FLIM/FRET techniques allow us to determine populations of interacting protein species on a point-by-point basis at each resolved voxel (volume element) in the cell[3].
Analysis of FRET between interacting proteins (i.e. intermolecular FRET) is often hampered by the dichotomy of interacting fraction of donor-accepter pairs. In a simple case, where all donors are bound to an acceptor, the donor fluorescence lifetime will have a single exponential lifetime. However, in a mixed population, where there is a distribution of molecular separations or unbound donor fluorophores, a multiple exponential decay kinetic is likely to be

* barber@gci.ac.uk; phone +44 1923 828-611; fax +44 1923 835-210; www.gci.ac.uk

observed. The presence of non-interacting species has a negative effect on the determination of FRET efficiency. A High FRET efficiency arising from a low concentration of interacting molecules may lead to the incorrect assumption that there is little or no interaction. If the protein interactions are localised to compartments below the imaging resolution, an averaging of the effect over the measured volume results and misinterpretation of the biological effects may result. Given appropriate data, analysis of the spatial distributions of fluorophores may be determined.
Thus the key to performing accurate and reliable FRET experiments by FLIM is robust fitting to the transient fluorescent intensity data that enables the extraction of the parameters of interest, e.g. lifetimes. It has been shown that global fitting algorithms can offer advantages over fitting each pixel transient of a FLIM image individually, these are:

- Faster computation
- More accurate fits with poor signal-to-noise ratio
- Better resolution of closely spaced lifetimes

These benefits have led us to develop a fast global fitting algorithm for the analysis of multi-exponential transient data.
The algorithm has been developed for the analysis of transient data generated by a FLIM system based on time-correlated single photon counting (TCSPC) which has been shown to be the most sensitive and direct technique, to date, for the measurement of lifetimes in the nanosecond timescale. One inherent aspect of TCSPC is the repetitive pulse nature of the excitation light which places an upper limit on the lifetimes that can be measured (as a significant number of molecules may be still to emit fluorescence when the next excitation pulse arrives). To explore this effect, an analytical model of this effect has been developed to generate simulated TCSPC data. Using this model we have analyzed the performance of the new global algorithm to this type of data.

2. MATERIALS AND METHODS

3.1. The TCSPC Model for Transient Generation

The starting point for the model of TCSPC generated transient data was a pure exponential decay.
If excited by a single delta function, a FRET sample may produce a signal of the form:

$$I(t) = Z + I_0(\alpha_1 \exp(-t/\tau_1) + \alpha_2 \exp(-t/\tau_2)) \quad (1)$$

If we extend this to an nth order exponential we can generalize to any number of interacting cell populations:

$$I(t) = Z + I_0 \sum_{i=1}^{n} (\alpha_i \exp(-t/\tau_i)) \quad (2)$$

In all cases, all the α_i sum to 1.0. The excitation laser in a TCSPC system produces a repetitive pulse excitation. The effect of which is that some signal may be left over from the pulses that have gone before. Let the pulses be separated by T seconds. For the single exponential function we can simply add in this effect by adding signal that started T seconds ago, and 2T seconds ago etc, if we make one assumption that the measurement will be made some time, after the sample is exposed to the laser pulse train, that is much greater than T.

$$I(t) = Z + I_0[\alpha \exp(-t/\tau) + \alpha \exp(-(t+T)/\tau) + \alpha \exp(-(t+2T)/\tau) + ...] \quad (3)$$

In general for the multiple exponential the index j can represent the contributions from previous pulses:

$$I(t) = Z + I_0 \sum_{i=1}^{n} \left[\sum_{j=0}^{\infty} \alpha_i \exp(-(t + jT)/\tau_i) \right] \quad (4)$$

The exponential function can be written as a product of two exponentials, one of which has no j dependence:

$$I(t) = Z + I_0 \sum_{i=1}^{n} \left[\left(\sum_{j=0}^{\infty} \exp(-jT/\tau_i) \right) . \alpha_i \exp(-t/\tau_i) \right] \quad (5)$$

There is an analytical solution to this infinite summation on j which is constant given T and τ_i. So we can write:

$$I(t) = Z + I_0 \sum_{i=1}^{m} R_i \alpha_i \exp(-t/\tau_i) \quad (6)$$

Where:

$$R_i = 1 + \frac{1}{\exp(T/\tau_i) - 1} \quad (7)$$

Several values were kept constant for all the simulated data: T = 12.2 ns (ca. 80 MHz repetition rate) and Z = 15 counts. A simulated instrument response function consisting of a Gaussian with a FWHM of 0.15 ns was convolved with the signal given by equation 6 and Gaussian noise was added with a standard deviation equal to the square root of the signal. This added noise approximates Poisson noise for signal amplitudes greater than 15 counts. A total signal of 10 ns duration was created with a delay of 2 ns before the excitation pulse to be sure to capture the rise of the transient and the background level before the peak of the fluorescence.

Three dimensional image stacks were created by this method to simulate FLIM data. A new random seed value was used to generate the noise for each pixel transient to ensure spatially independent noise characteristics. Images were 128 by 128 pixels in size, each pixel holding a 256-time-point 16-bit-integer transient spanning 10 ns. Mono-exponential and bi-exponential images were created using τ, α and I_0 values that were constant within individual images. These images were used to analyse the performance of the algorithm by performing single pixel fits at every pixel or by splitting the images up into 16 32-by-32-pixel squares on which global analysis could be performed. The variation between these 16 patches giving an indication of the random error in the determination of global parameters.

3.2. Analysis of Fluorescence Lifetime Imaging Data for FRET

Quantifying the interacting sub-population of proteins is one of the main aims of an intermolecular FRET experiment. FRET, when performed by fluorescence lifetime measurement of the donor species, results in data that may reflect both interacting and non-interacting protein populations. These two populations are distinct in their decay kinetics and usually a bi-exponential transient results.

The degree of interaction between these molecules can be quantified by the FRET efficiency. This value will depend on the molecule separation and in general there will be a distribution of separations resulting in a complicated transient signal. It would be most appropriate to consider application of a complex distributed lifetime model to the experimental data in order to recover the distance distribution of fluorophores, as has been demonstrated by Rolinski *et al.*[4]. However, given the complexity of this approach, the need for extremely high photon counts to achieve statistically relevant results and the almost on/off nature of the 6th power dependence on separation[5], we assume that only two populations of donor molecules are present, i.e. interacting and non-interacting populations. A bi-exponential fluorescence decay model is assumed in order to determine the fluorescence lifetime of non-interacting and interacting sub-populations. The data was fitted by iterative convolution (IC) to:

$$I(t) = Z + I_0 \int_{-\infty}^{\infty} I_{instr}(t - t').\left(\alpha_1 \exp(-t/\tau_1) + \alpha_2 \exp(-t/\tau_2)\right) dt' \quad (8)$$

Where $I_{instr}(t)$ is the instrumental response, I_0 the peak intensity, α_1 and α_2 are the fractional proportions of the lifetimes, τ_1 and τ_2 respectively. IC is the most robust method for use on data that contains a significant noise component. The reduced goodness-of-fit parameter, χ_r^2, was used[5]:

$$\chi_r^2 = \frac{\sum_{k=1}^{n} \frac{[I(t_k) - I_c(t_k)]^2}{I(t_k)}}{n - p} \quad (9)$$

where $I(t_k)$ is the data and $I_c(t_k)$ the fit value at the k^{th} time point, t_k. n is the number of time points and p the number of variable fit parameters. χ_r^2 is minimised using a modified Marquardt algorithm and compared alongside plots for the weighted residuals ($R = (I(t_k) - I_c(t_k))/I(t_k)$) to determine the validity of the decay model.

In the analysis of FRET data (particularly for protein-interaction applications) there are usually two elements that must be considered, interacting fluorophore population and FRET efficiency. Bulk measurements of FRET efficiency (i.e.

intensity based methods) cannot distinguish between an increase in FRET efficiency (i.e. coupling efficiency) and an increase in FRET population (concentration of FRET species), since the two parameters are not resolved. Measurements of FRET, based on analysis of the fluorescence lifetime of the donor may resolve this dichotomy when analysed using multi-exponential decay models. The assumption that non-interacting and interacting fractions are present allows us to determine both the efficiency of interaction (i.e. from τ_1) and the fractional population of interacting population (i.e. α_1).

3.3. Global Analysis of Time-domain Imaging Data

Previously FLIM images have been analyzed by treating each pixel of the image independently, attempting to fit the fluorescence decay transient with a multi-exponential or stretched exponential fit. In global analysis, on the other hand, we assume that there are fixed lifetimes for the fluorophores across the image or between images and attempt to determine these global values. The most straightforward way of finding global values is to fit each transient and then to take an average of the fitted lifetimes, but this suffers in that no distinction is made between transients which exhibited a good fit (low χ^2 value) and those which did not. A better method is to fit the entire data set simultaneously; this is global analysis[6].

In this part of the paper the mathematical and computational aspects of this analysis are outlined, with a more detailed treatment in appendix A. Global analysis for multi-exponential fitting, where we are attempting to find global lifetime values, can be made far more computationally efficient than fitting each individual transient and then averaging the results; an unusual case where achieving better quality results is actually faster.

Appendix A describes our global algorithm in general terms but in order to describe the specific task of analysis of FLIM data, we assume that we are performing a bi-exponential fit; everything in this section applies equally to multi-exponential fits with a different number of exponentials, with the obvious changes. Let us assume there are N transients, where the rth transient has data $(t_i, I_i^{(r)})$; note that the time data is the same for each transient. We fit with the following model:

$$I = f(t;\tau_1,\tau_2;Z,A_1,A_2) = Z + A_1\exp(-t/\tau_1) + A_2\exp(-t/\tau_2) \tag{10}$$

where we wish to fit the lifetimes (τ_1 and τ_2) globally, and the amplitudes ($A_1 = \alpha_1.I_0$, $A_2 = \alpha_2.I_0$) and background (Z) locally. For each transient, s, and exponential order, k (k = 2 for bi-exponential), the corresponding partial derivatives can be calculated:

$$\begin{aligned}
\frac{\partial f\left(t_i;\tau_1,\tau_2;Z,A_1^{(s)},A_2^{(s)}\right)}{\partial Z} &= 1 \\
\frac{\partial f\left(t_i;\tau_1,\tau_2;Z,A_1^{(s)},A_2^{(s)}\right)}{\partial A_k^{(s)}} &= \exp(-t_i/\tau_k) \\
\frac{\partial f\left(t_i;\tau_1,\tau_2;Z,A_1^{(s)},A_2^{(s)}\right)}{\partial \tau_k} &= \frac{A_k^{(s)}t}{\tau_k^2}\exp(-t_i/\tau_k)
\end{aligned} \tag{11}$$

It is important to note that most of these values can be calculated once and then used repeatedly for each transient; in particular, we calculate and store the values of $\exp(-t_i/\tau_k)$ and $\left(t/\tau_k^2\right)\exp(-t_i/\tau_k)$ for each i and k, allowing much of the calculation by additions and multiplications only. This makes global analysis very efficient in this case, far more so than fitting each transient independently, which requires calculation of all the exponentials for each transient.

Up to this point we have ignored the instrumental response of the apparatus. Assuming a linear response, we manage this by convolving the measured instrument response with the fitting function before attempting the Marquardt algorithm. Performing a per-transient analysis requires a computationally expensive convolution for each transient, however, for global analysis (since convolutions are linear) we may convolve once only with the raw exponential decays (mentioned above), meaning that we perform a total of only four convolutions instead of one per-transient for each optimisation step. Again this provides a significant computational saving.

Finally, this algorithm can be modified in a straightforward manner for multiprocessor or distributed machines, although the time-savings will not necessarily be too significant: since most calculations are performed on a per-transient basis,

this task could be distributed by transient, then gathering the data back together to determine the proposed global change in parameters.

2.3.1. Initial Parameter Estimation

The speed of convergence of the Marquardt algorithm is dependant on the initial guess of parameter values (or starting values) that are fed to the algorithm. In this work we have based the starting values on a triple-integral fit to the data, which is performed by integrating the transient signal within 3 equal time windows. Estimated Z, I_0 values and a single average τ value can be calculated from the 3 integrals using the rapid lifetime determination (RLD) method[7].

The global τ values are estimated by summing all the transients in the image together and firstly performing a triple integral fit. This provides an estimated Z, I_0 and a single τ_{est}. Suitable proportions are chosen for the α_i and τ_i values in multiple exponent fits (Bi-exponential fits use: $\alpha_1=3/4$, $\alpha_2=1/4$, $\tau_1=\tau_{est}$, $\tau_2=2/3.\tau_{est}$ and Tri-exponential fits use: $\alpha_1=2/3$, $\alpha_2=1/6$, $\alpha_3=1/6$, $\tau_1=\tau_{est}$, $\tau_2=2/3.\tau_{est}$, $\tau_3=1/3.\tau_{est}$). These are used to estimate all parameters for a Marquardt optimised fit of the summed data, over the whole image, which provides a good estimate of all the global variables.

A estimate of all the local variables is then sought by performing a triple integral fit on each pixel transient followed by a Marquardt optimised fit. Significant time savings can be made here because suitable global τ values have already been determined we can calculate the exponential parts and convolve each with the instrument response in advance.

2.5. Lifetime Invariant Fitting

An alternative to global fitting is lifetime invariant fitting. In this method the global parameters, the lifetimes (which are invariant), are obtained from summing all the transients together and fitting this summed transient. The lifetime values obtained in this way can be compared with the results of global analysis. Since a lifetime invariant step is always the first step in our global analysis algorithm, we expect a global fit to never be worse than a lifetime invariant fit.

3. RESULTS AND DISCUSSION

3.4. Comparison between Localised and Global Analyses using Modelled Data

Data was generated using the repetitive excitation model to test the global algorithm against single pixel fits and lifetime invariant fits. Figure 1 shows example mono-exponential transients from the model together with example fits.

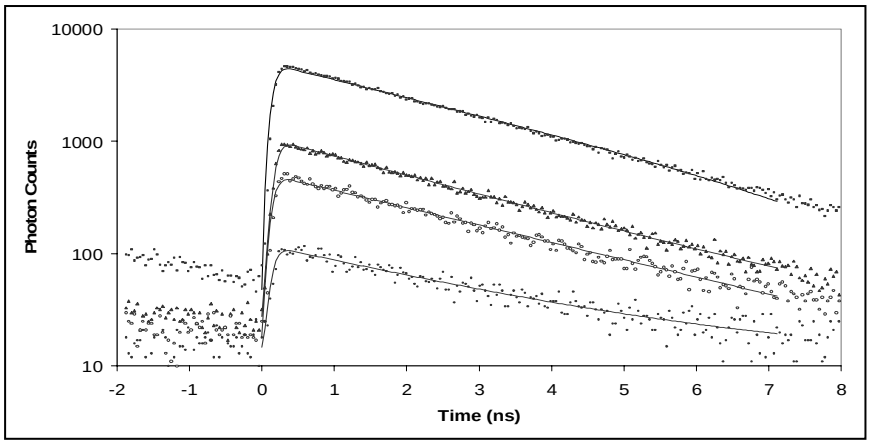

Figure 1: Example mono-exponential transients generated by the repetitive excitation TCSPC model. Transients with peak counts (I_0) of 100, 500, 1000 and 5000 photons are shown together with example Marquardt optimised fits (solid lines). In each case Z = 15 counts and τ = 2.5 ns were used to generate the data. Note the pre-pulse signal far above the background level at time<0.

We can see from figure 2 that individual pixel and global fits consistently underestimate the lifetime for values greater than 2 ns. This is due to the effect of repetitive excitation. Most of the fitting error occurs at the start of the transient because the background value has been elevated and disturbs the true form of the transient rise. If the true background level is known and fixed for fitting, the situation is slightly improved but we are still not able to fit the data before the peak of the transient. The problem can be circumvented by relaxing the requirement to fit the rise of the transient. This may seem counterintuitive as, if our model is correct, we would want to use as much of the data as possible but the effect of repetitive excitation invalidates the model.

To exclude the rise of the transient the starting point of valid data (t = 0) was set to minimise the χ^2 off a single exponential fit. This was found to be 0.36 ns after the point of steepest rise for the simulated data and just excludes the rise of the transient from the fit. This process has been implemented to automatically estimate this point for real data.
Figure 3 repeats the format of figure 2 but shows the results of excluding the transient rise from the fit. We can see that the systematic lifetime under-estimation has been removed. Figure 3b shows that with global or invariance fitting of a 32x32 pixel area, the error in extracted lifetime can be lower than 0.4 % for signals with a peak of 500 photon counts or more, over the range 0.1 – 10.0 ns (Note the change in y-scale between figures 3a and 3b). The accuracy of extracting the amplitude and the χ^2 is shown in figure 4. The global χ^2 was usually in the range 1.00 to 1.04.
Taking this further, Figure 5 shows how at longer lifetimes and systematic error in lifetime recovery remains small but the random error becomes excessively large.
Arguments could be made against the need to convolve with the instrument function if the need to fit the rise of the data is removed. In additional experiments it was found that without convolving the excitation function at all, the lifetime is always over estimated because the convolution will tend to lengthen the transient.

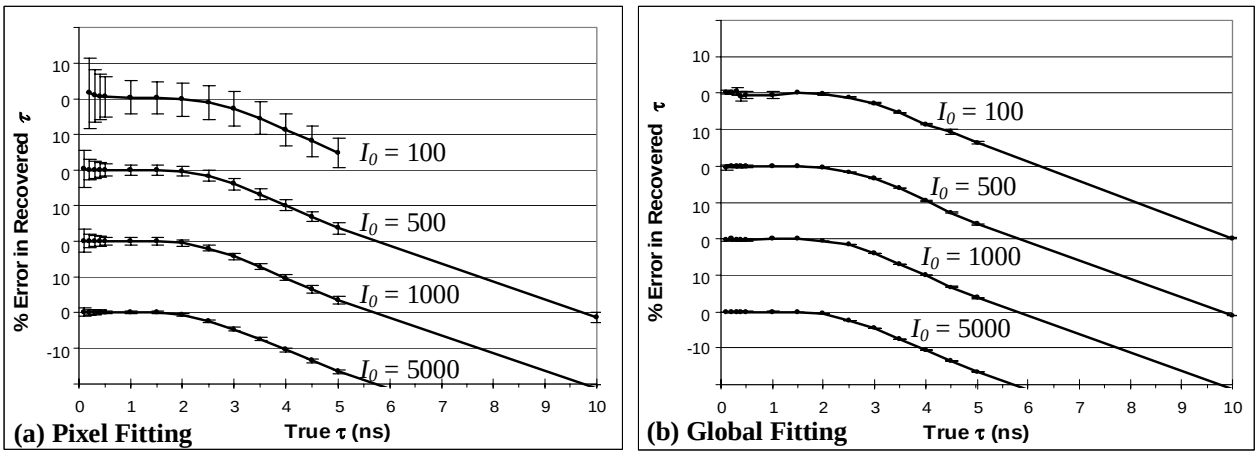

Figure 2: The error in the lifetime recovered from simulated single exponential data by individual pixel fits (a) and by global fitting (b). Four plots are shown on each graph for different peak photon counts (I_0). The error bars show the standard deviation in measurements over the 128 by 128 pixel image (a) or over 16 patches of 32 by 32 pixels (b).

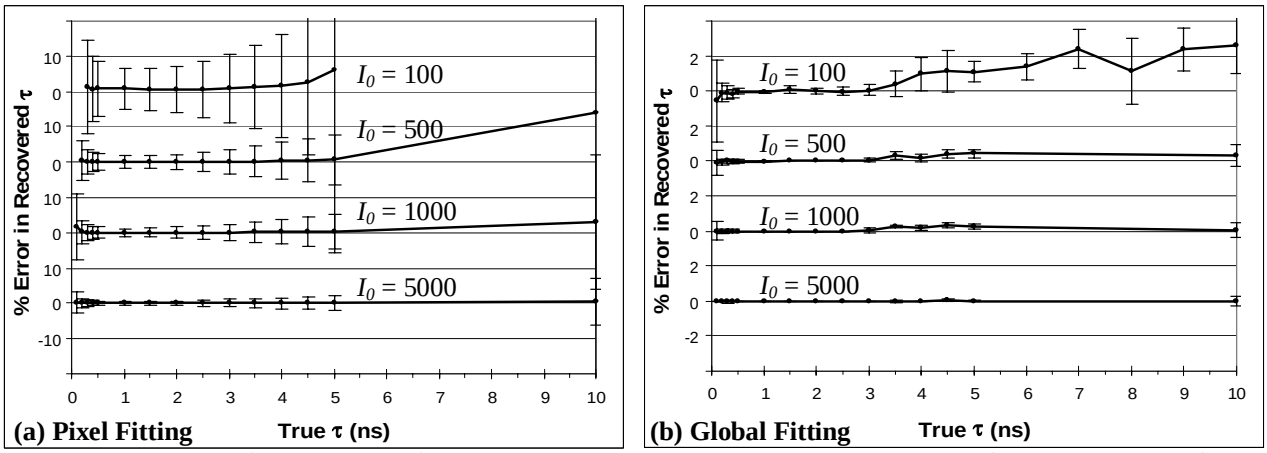

Figure 3: The error in lifetime recovered from simulated single exponential data by individual pixel fits (a) and by global fitting (b) with the rise of the transient excluded. Four plots are shown on each graph for different peak photon counts (I_0). The error bars show the standard deviation in measurements over the 128 by 128 pixel image (a) or over 16 patches of 32 by 32 pixels (b).

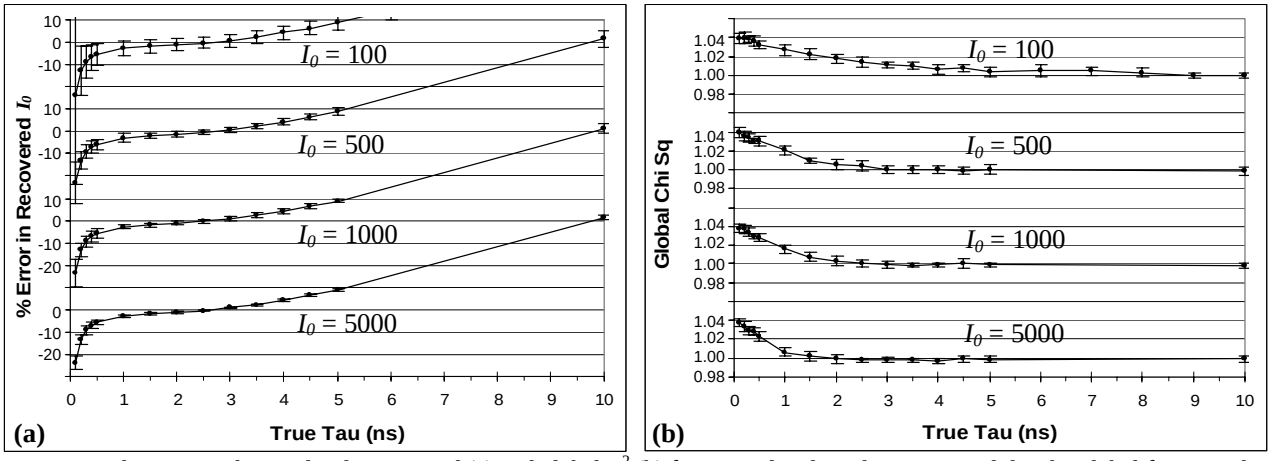

Figure 4: The error in the amplitude recovered (a) and global ψ^2 (b) from simulated single exponential data by global fitting with the rise of the transient excluded. Four plots are shown on each graph for different peak photon counts (I_0). The error bars show the standard deviation in measurements over 16 patches of 32 by 32 pixels.

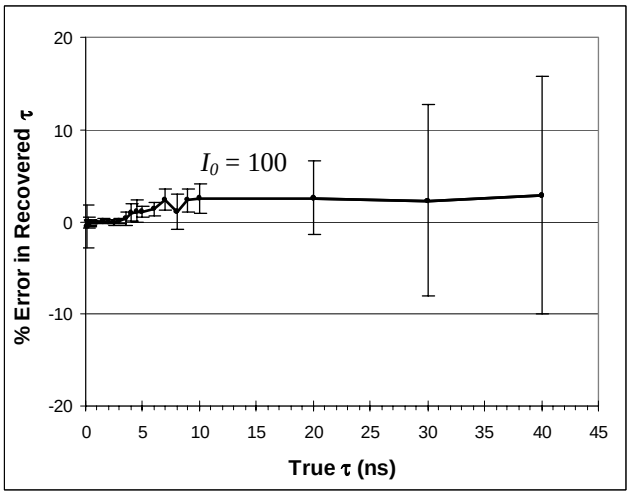

Figure 5: The error in recovered τ from longer lifetime mono-exponential transients by global fitting for a peak photon count of 100. The error bars show the standard deviation in measurements over 16 patches of 32 by 32 pixels. The modelled data included a ca. 12 ns repetitive excitation.

3.5. Simulated FRET Data

To simulate FRET data a bi-exponential decay was modelled with τ_1 equal to 2.15 ns, approximately corresponding to a fluorescent emission by GFP. We modelled different peak counts and different proportions of τ_1 and τ_2. The normal course of events in a lifetime FRET experiment may be to measure the lifetime of the non-interacting donor in a control sample. This lifetime can then be fixed as a parameter in fitting of experimental bi-exponential data. The results of which are used to determine FRET efficiency for example. This procedure was followed with the test data which resulted in Figure 6. Figure 6a demonstrates that the lifetime of the interacting population (τ_2) can be accurately determined, with a peak photon count of 500 or more, over a range of interacting lifetimes and population sizes. An interacting population of 10% could be accurately characterised as long as its lifetime was below 1 ns. Figure 6b shows that there is a greater error in extracting the population amplitudes and indeed there was great difficulty in this if the lifetime of the interacting population was above 1.6 ns.

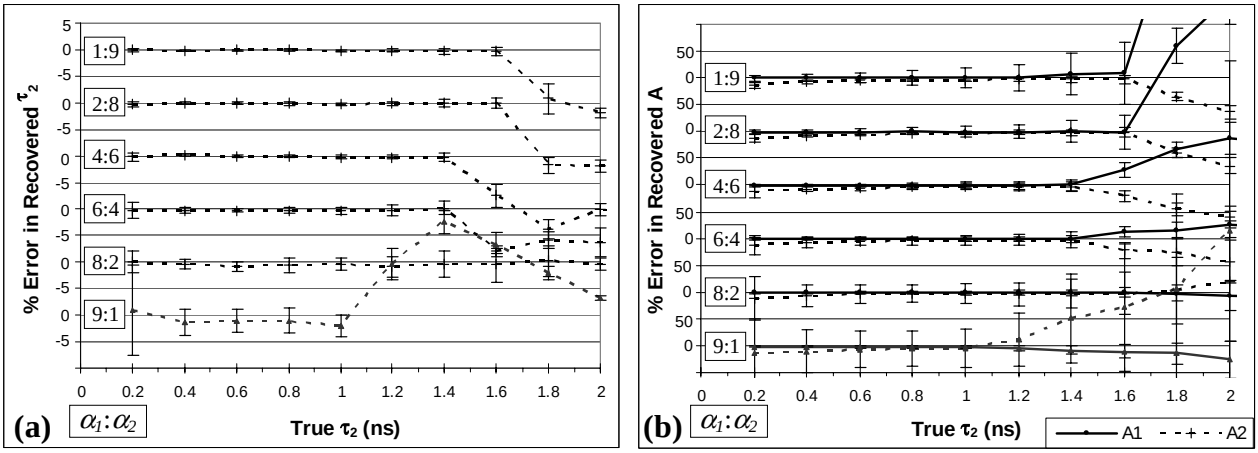

Figure 6: The error in the lifetime (a) and amplitude recovered (b) from simulated bi-exponential data by global fitting with the rise of the transient excluded. Six plots are shown on each graph for different ratios of interacting and non-interacting populations (α_1:α_2), I_0 = 500. The error bars show the standard deviation in measurements over 16 patches of 32 by 32 pixels.

In order to explore the sensitivity to the fixed lifetime of the non-interacting population (τ_1), figure 7 shows an example χ^2 surface, or support plane, for a global fit of bi-exponential test data (τ_1 = 2.15 ns, τ_2 = 0.8 ns, α_1:α_2 = 6:4, I_0 = 500). The surface demonstrates a clear single minimum at the true values, as part of a curved valley. This shows that although the correct value gives clearly the best fit as is to be expected, small variations in the fixed value of τ_1 will also produce good robust results. Further studies of the support planes showed that the parameter sensitivity shifts towards the more dominant population, as may be expected. In real experiments where it may be difficult to determine the lifetime of the non-interacting population it may be useful to "restrain" the τ_1 value to a range (2.0 to 2.3 ns for example). This type of restrained fitting allows an increased optimisation of the fit with experimental as well as control data.

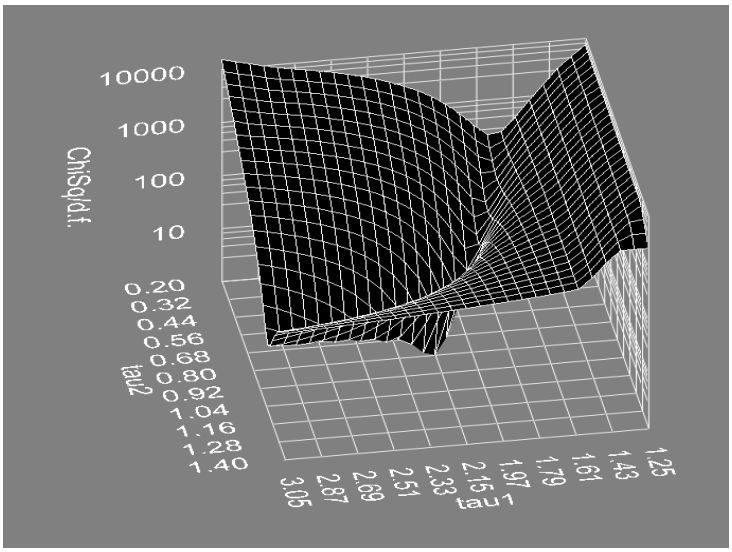

Figure 7: The χ^2 surface, or support plane, for global fit of bi-exponential test data (τ_1 = 2.15 ns, τ_2 = 0.8 ns, α_1:α_2 = 6:4, I_0 = 500). Note the curved valley ranging from $\tau_1 \approx 3.0$, $\tau_2 \approx 1.3$ ns to $\tau_1 \approx 1.8$, $\tau_2 \approx 0.2$ ns.

3.6. Processing Time

The global fitting algorithm is extremely efficient and is significantly faster the performing single fits on a per pixel basis. Timings were made on a 32 by 32 pixel region (500 peak count) of bi-exponential data with either global fitting or individual pixel fits of the same region. The results are presented in table 1. Tests were performed on two computers housing different processors: a Pentium® 4 by Intel® (Santa Clara, CA, USA) running at a clock speed of 2.4 GHz, and an Athlon™ 2600+ by AMD (Sunnyvale, CA, USA) with a clock speed of 2.1 GHz. The much lower processing time required by the AMD based processor is thought to be due to its increased floating-point operation performance.

Table 1: Processing times for the global analysis algorithm and individual pixel fits on bi-exponential data.

	Individual pixel fits	***Global fit***
Intel® Pentium® 4 2.5 GHz	15 seconds	1.5 seconds
AMD Athlon™ 2600+	4 seconds	< 1 second

4. CONCLUSION

An algorithm for the global analysis of time resolved data from a FRET experiment has been presented and its performance analysed. The algorithm was tested by the simulation of data with an analytical model of TCSPC generated signals. This model included the effect of a repetitive excitation signal and was able to generate both single and bi-exponential transients with added Poisson noise.

The results show that the effects of the repetitive excitation (at *ca.* 12 ns) preclude accurate lifetime determination if data before the peak of the transient is included in the fit. If this rise time is excluded, the accurate extraction of populations with lifetimes in the range 0.1 to 10 ns is possible, even when these effects are not represented in the fitting algorithm. Extracting longer lifetimes is possible but with an increasing random error. Data from a FRET experiment was simulated with bi-exponential transients comprising interacting and non-interacting populations. The proportion of interacting population was varied from 10 % to 90%, and with a lifetime varied from 0.2 to 2.0 ns, in the presence of a fixed lifetime non-interacting population (2.15 ns). The error in extracting the lifetime of the interacting population was as low as 0.4% if the transient contains a peak of more than 500 photons and its lifetime was below 1 ns. There was a much greater error in extracting the relative amplitudes and indeed there was great difficulty in this if the lifetime of the interacting population was above 1.6 ns. Future studies may show that the results may be improved by including the repetitive excitation in the fitting model.

ACKNOWLEDGEMENTS

We gratefully acknowledge the continuing collaboration with M. Parsons and T. Ng of Kings College London. This work was supported by Cancer Research UK and by the UK Research Councils Basic Technology Programme.

APPENDIX A

We begin describing global analysis by making no assumptions about the type of data being processed or the nature of the fitting function. We assume that we have a collection of N data sets, where the r^{th} data set has data points $(x_i^{(r)}, y_i^{(r)})$, with $i = 1,2, \ldots, n_r$. In the case of FLIM, all the measurements are made at the same time intervals, i.e. $t_1, t_2, \ldots, t_n$, so that we can let $n_r = n$ and $x_i^{(r)} = t_i$.

Assume a fitting function of the form

$$y = f(x; \mathbf{a}, \mathbf{b}) \tag{A1}$$

where $\mathbf{a} = (a_1,\ldots,a_p)$ are the parameters which are to be fitted globally and $\mathbf{b} = (b_1,\ldots,b_p)$ are the parameters which are to be fitted locally, that is, independently for each data set. For example, f could be the bi-exponential function:

$$f(x; a_1, a_2; b_1, b_2, b_3) = b_1 + b_2 \exp(-x/a_1) + b_3 \exp(-x/a_2) \tag{A2}$$

here, we are globally fitting the lifetimes (a_1 and a_2, normally called τ_1 and τ_2), while all other parameters are being fit on a per-data-set basis.

The task is then to minimise the global χ^2 value, given by

$$\chi^2 = \sum_{r=1}^{N} \sum_{i=1}^{n_r} \left[\frac{y_i^{(r)} - f\left(x_i^{(r)}; \mathbf{a}; \mathbf{b}^{(r)}\right)}{\sigma_i^{(r)}} \right]^2 \tag{A3}$$

with $\mathbf{b}^{(r)}$ being the values of the **b** parameters for the r^{th} data set and $\sigma_i^{(r)}$ the standard deviation of the error of the i^{th} data point of the r^{th} data set. This is now a standard problem of non-linear least squares fitting, which can be handled by the Marquardt algorithm. The difficulty is that we have to potentially handle a very large number of parameters; for the example of a bi-exponential decay we have two global parameters and three local parameters for *each data set*. For a 128 x 128 pixel FLIM image, this amounts to just over 49,000 parameters.

Before describing an efficient method for overcoming this obstacle, we first recall some of the key components of the Marquardt algorithm[7]; where we have a set of data (x_i, y_i) and we fit with a function $y = f(x_i;\mathbf{a})$. We set

$$\alpha_{kl} = \sum_i \frac{1}{{\sigma_i}^2} \cdot \frac{\partial f(x_i;\mathbf{a})}{\partial a_k} \frac{\partial f(x_i;\mathbf{a})}{\partial a_l} \tag{A4}$$

and

$$\beta_k = \sum_i \frac{y_i - f(x_i;\mathrm{a})}{{\sigma_i}^2} \cdot \frac{\partial f(x_i;\mathrm{a})}{\partial a_k} \tag{A5}$$

then multiplying the diagonal elements in the matrix $[\alpha_{kl}]$ by a factor $1 + \lambda$ for an appropriate λ gives us the matrix $[\alpha'_{kl}]$. A step of the Marquardt algorithm requires us to solve the set of linear equations

$$\sum \alpha'_{kl} \delta a_l = \beta_k \tag{A6}$$

to find the suggested change in the parameters **a**. Note that both $[\alpha_{kl}]$ and $[\alpha'_{kl}]$ are symmetric.
In the case in point, there are two types of parameter, so there are four parts to the alpha matrix. Firstly, if both parameters chosen are global, we have

$$\alpha(a_k, a_{k'}) = \sum_{r=1}^{N} \sum_{i=1}^{n_r} \frac{1}{\left(\sigma_i^{(r)}\right)^2} \cdot \frac{\partial f\left(x_i^{(r)};\mathbf{a};\mathbf{b}^{(r)}\right)}{\partial a_k} \cdot \frac{\partial f\left(x_i^{(r)};\mathbf{a};\mathbf{b}^{(r)}\right)}{\partial a_{k'}} \tag{A7}$$

Note that every data set contributes to this sum, as a_k and $a_{k'}$ are parameters for each data set. Next if one parameters is global and another is local (and it does not matter which way around, by symmetry), we have

$$\alpha\left(b_k^{(s)}, a_{k'}\right) = \sum_{r=1}^{N} \sum_{i=1}^{n_r} \frac{1}{\left(\sigma_i^{(r)}\right)^2} \cdot \frac{\partial f\left(x_i^{(r)};\mathbf{a};\mathbf{b}^{(r)}\right)}{\partial b_k^{(s)}} \cdot \frac{\partial f\left(x_i^{(r)};\mathbf{a};\mathbf{b}^{(r)}\right)}{\partial a_{k'}} \tag{A8}$$

Since the first partial derivative is zero unless $r = s$, this reduces to a single summation

$$\alpha\left(b_k^{(s)}, a_{k'}\right) = \sum_{i=1}^{n_s} \frac{1}{\left(\sigma_i^{(s)}\right)^2} \cdot \frac{\partial f\left(x_i^{(s)};\mathbf{a};\mathbf{b}^{(s)}\right)}{\partial b_k^{(s)}} \cdot \frac{\partial f\left(x_i^{(s)};\mathbf{a};\mathbf{b}^{(s)}\right)}{\partial a_{k'}} \tag{A9}$$

Finally, if both parameters are local, we have, by the same argument, $\alpha\left(b_k^{(s)}, b_{k'}^{(s')}\right) = 0$ unless $s = s'$, in which case we have

$$\alpha\left(b_k^{(s)}, b_{k'}^{(s)}\right) = \sum_{i=1}^{n_s} \frac{1}{\left(\sigma_i^{(s)}\right)^2} \cdot \frac{\partial f\left(x_i^{(s)};\mathrm{a};\mathrm{b}^{(s)}\right)}{\partial b_k^{(s)}} \cdot \frac{\partial f\left(x_i^{(s)};\mathrm{a};\mathrm{b}^{(s)}\right)}{\partial b_{k'}^{(s)}} \tag{A10}$$

Handling the β vector is similar but simpler, since there is only one partial derivative. We can now sketch the α matrix; we arrange the rows and columns so that the global variables appear first, followed by the local variables ordered by data set:

$$\left(\begin{array}{c|ccccc} \mathbf{P} & \mathbf{Q_1} & \mathbf{Q_2} & \mathbf{Q_3} & \cdots & \mathbf{Q_N} \\ \hline \mathbf{R_1} & \mathbf{S_1} & \mathbf{0} & \mathbf{0} & \vdots & \mathbf{0} \\ \mathbf{R_2} & \mathbf{0} & \mathbf{S_2} & \mathbf{0} & \vdots & \mathbf{0} \\ \mathbf{R_3} & \mathbf{0} & \mathbf{0} & \mathbf{S_3} & \vdots & \mathbf{0} \\ \vdots & \cdots & \cdots & \cdots & \ddots & \vdots \\ \mathbf{R_N} & \mathbf{0} & \mathbf{0} & \mathbf{0} & \cdots & \mathbf{S_N} \end{array}\right) \tag{A11}$$

In this matrix, **P** contains the entries for $\alpha(a_k, a_{k'})$, where both components are global; $\mathbf{Q_s}$ and $\mathbf{R_s}$ contain the entries for $\alpha\left(a_k, b_{k'}^{(s)}\right)$ and $\alpha\left(b_{k'}^{(s)}, a_{k'}\right)$ (note that $\mathbf{R_s}$ is the transpose of $\mathbf{R_s}$ by symmetry), and $\mathbf{S_s}$ contains the entries for $\alpha\left(b_k^{(s)}, b_{k'}^{(s)}\right)$. The α' matrix is identical except that the diagonal elements have been scaled by 1 + λ, so the zero entries remain zero and the matrix remains symmetric. Note that the α and α' matrices are doubly bordered block diagonal and have the general form:

$$\left(\begin{array}{c|c} \mathbf{P} & \mathbf{Q} \\ \hline \mathbf{R} & \mathbf{S} \end{array}\right) \tag{A12}$$

Since we need to solve the equations corresponding to (A12) as the next step in our process, we can do this by taking the inverse of the α' matrix (Numerical instability is not important here; essentially we are only finding an approximate next step for the parameters; if we are very inaccurate, this will be rejected and larger values of λ will give more stable matrices). The inverse is [7]

$$\left(\begin{array}{c|c} \tilde{\mathbf{P}} & \tilde{\mathbf{Q}} \\ \hline \tilde{\mathbf{R}} & \tilde{\mathbf{S}} \end{array}\right) \qquad \text{where:} \qquad \begin{aligned} \tilde{\mathbf{P}} &= \left(\mathbf{P} - \mathbf{Q}\cdot\mathbf{S}^{-1}\cdot\mathbf{R}\right)^{-1} \\ \tilde{\mathbf{Q}} &= -\left(\mathbf{P} - \mathbf{Q}\cdot\mathbf{S}^{-1}\cdot\mathbf{R}\right)^{-1}\cdot\left(\mathbf{Q}\cdot\mathbf{S}^{-1}\right) \\ \tilde{\mathbf{R}} &= -\left(\mathbf{S}^{-1}\cdot\mathbf{R}\right)\cdot\left(\mathbf{P} - \mathbf{Q}\cdot\mathbf{S}^{-1}\cdot\mathbf{R}\right)^{-1} \\ \tilde{\mathbf{S}} &= \mathbf{S}^{-1} + \left(\mathbf{S}^{-1}\cdot\mathbf{R}\right)\cdot\left(\mathbf{P} - \mathbf{Q}\cdot\mathbf{S}^{-1}\cdot\mathbf{R}\right)^{-1}\cdot\left(\mathbf{Q}\cdot\mathbf{S}^{-1}\right) \end{aligned} \tag{A14}$$

Thus, global analysis using the Marquardt algorithm is essentially straightforward and computationally feasible, both from the aspect of speed and of storage.

REFERENCES

1. Ng T, Squire A, Hansra G, Bornancin F, Prevostel C, Hanby A, Harris W, Barnes D, Schmidt S, Mellor H, Bastiaens PIH and Parker PJ (1999). Imaging PKC alpha activation in cells. *Science*, **283**, pp2085-2089.
2. Wouters FS, Verveer PJ and Bastiaens PIH (2001). Imaging Biochemistry inside cells. *Trends Cell Biol.* **11**(5), pp203-211.
3. Becker W, Benndorf K, Bergmann A, Biskup C, König K, Tirplapur U and Zimmer T (2001). FRET measurements by TCSPC laser scanning microscopy. *Proc. SPIE* **4431**, pp414-419.
4. Rolinski OJ, Birch DJS, McCartney LJ and Pickup JC (2000). A method of determining donor–acceptor distribution functions in Förster resonance energy transfer. *Chem. Phys. Lett.* **324**, pp95-100.
5. Lakowicz JR, Principles of fluorescence spectroscopy. Kluwer Academic/Plenum Publishers, ISBN 0-306-46093-9.
6. Verveer PJ, Squire A, Bastiaens PIH (2001). Global analysis of fluorescence lifetime imaging data. *Biophys. J.* **78**, pp2127-2137.
7. Sharman, K. K., Periasamy, A., Ashworth, H., Demas, J. N. and Snow, N. H. "Error Analysis of the Rapid Lifetime Determination Method for Double-Exponential Decays and New Windowing Schemes." Anal. Chem. **71**, 947-952 (1999).
8. W. H. Press, S. A. Teukolsky, W. T. Vetterling and B.P. Flannery (1992). Numerical Recipes in C, 2nd edition, *Cambridge University Press.*